

TECHNICAL ARTICLE

Influence of Titanium Additions to Aluminum on the Microhardness Value and Electrochemical Behavior of Synthesized Aluminum-Titanium Alloy in Solutions of HCl and H₃PO₄

Abdel-Rahman El-Sayed, Adila E. Mohamed, Fatma S.M. Hassan, and Mohamed Sarwat El-Mahdy

Submitted: 5 December 2021 / Revised: 9 March 2022 / Accepted: 16 April 2022 / Published online: 31 August 2022

The effect of Ti content in various concentrations as an alloying element with Al on both microhardness and crystallization structure of aluminum–titanium alloys was studied, utilizing x-ray diffraction (XRD) and a scanning electron microscope (SEM). To study the electrochemical and corrosion performance of Al and its investigated alloys in 0.5 M solutions of HCl and H₃PO₄, two different techniques were used: extrapolation of Tafel plot and electrochemical impedance spectroscopy (EIS). Tafel plots and EIS revealed a similar trend. Generally, the rate of corrosion of the alloys was higher than that of Al. This investigation exhibited that the corrosion of Al alloying with Ti increased with an increase in both Ti content and temperature, which is due to reducing the growth of oxide film on the surface. Changes in the standard values of both entropy (ΔS) and enthalpy (ΔH), in addition to apparent activation energy (E_a) of corrosion processes of Al and its alloys in HCl and H₃PO₄, were evaluated. The evaluated data indicated negative values of ΔS , while the values of ΔH were positive. Besides, the decrease in ΔH value with the increase of Ti content in the alloy revealed that the dissolution of the studied alloys was fast. The positive values of ΔH were accompanied by an endothermic process. On the other hand, the activation energy (E_a) was decreased as a result of Al alloying with Ti in the two mentioned acids. Those results were supported by the corrosion current density (i_{corr}) and impedance parameters. By comparing the data obtained for both HCl and H₃PO₄ in all investigated electrodes, the corrosion current density (i_{corr}) in H₃PO₄ was lower than that in HCl. Such behavior can be ascribed to the aggressive attack of Cl⁻ ions on the surfaces of the investigated electrodes, leading to pits formation.

Keywords aluminum-titanium alloy, corrosion, EIS, hydrochloric and phosphoric acid, microhardness, tafel polarization

1. Introduction

Due to their technical significance and industrial applications, studies on the dissolution and stability of aluminum and its alloying with many elements have been of primary interest, especially for the aviation and automotive industries, and manufacture of containers, household appliances, and electronic devices (Ref 1, 2). Aluminum is a soft metal that is thermally and mechanically stable and is often alloyed to enhance its other properties, such as high electrical properties, resistance to fatigue, high strength, recyclability, and thermal conductivity (Ref 3-5).

Some elements, such as Zn, Ti, Hg, and In, were added to Al in order to activate it and to be used as an anode in batteries

(Ref 6, 7). Schreiber and Reding (Ref 8) reported that Al anode retained 95% performance as relatively negative potential after adding Zn and Hg to Al. Al₃Ti/Al composite was prepared by the melt of solid powders, employing the direct reaction between solid titanium powder or a titanium product in certain salts and aluminum. The mentioned composite had many advantages, including strong wet ability and a clean interface between the reinforcement and the Al matrix (Ref 9).

H₃PO₄, an important industrial acid, was utilized in the synthesis of semiconductors and boards of the printed circuit in the electronics industry (Ref 10). In the food industry, pure H₃PO₄ was used. Phosphoric acid (additive E338) was utilized to acidify foods and drinks, including colas and jams, to give them a tangy or sour flavor. Soft drinks that contain phosphoric acid, such as Coca-Cola, are known as phosphate sodas or phosphates (Ref 11). It was also used in the treatment of water and the removal of mineral particles from process machinery and boilers. For aluminum refractory, it served as a binder. Phosphoric acid was commonly used in the acid-cleaning aluminum and Al electropolishing (Ref 12) while still showing a strong corrosive action on aluminum and its alloys. Solutions of HCl were used for chemical and electrochemical etching and pickling of Al (Ref 13).

Many recent studies have shown a particular interest in adding titanium to the aluminum matrix. This is due to the

Abdel-Rahman El-Sayed, Department of Chemistry, Faculty of Science, Sohag University, Sohag 82524, Egypt; Adila E. Mohamed, Fatma S.M. Hassan, and Mohamed Sarwat El-Mahdy, Department of Chemistry, Faculty of Science, Aswan University, Aswan 81528, Egypt. Contact e-mail: elsayed777@yahoo.com.

formation of Al₃Ti phases, which are promising reinforcement of the aluminum matrix because of their high modulus, low density, excellent specific strength, wear resistance, and high-temperature rigidity (Ref 14-16). Consequently, extensive attention has been paid to the in situ Al₃Ti/Al alloy, and various methods have been developed, such as in situ casting (Ref 17), powder metallurgy (Ref 18), processing of friction stirs (Ref 19), and mechanical alloying (Ref 20).

The present work aimed at the fabrication of four new Al-wt.%Ti alloys with various Ti concentrations as shown in Table 1, and it is expected that the chosen percentages of Ti in the studied alloy are soluble in the Al matrix. Besides, the microhardness of aluminum and its alloys were studied using Vickers microhardness. This research also intended to estimate the Ti effect on the processes of corrosion for the studied samples in phosphoric and hydrochloric acid solutions. Corrosion tests included Tafel polarization and EIS measurements. Furthermore, the study expected to reveal the effect of temperature on the samples. XRD and SEM-EDAX were utilized to characterize the synthesized alloy containing various contents of Ti before and after electrochemical measurements. Based on the data obtained, the corrosion resistance of the investigated samples was discussed and compared.

2. Experimental Procedure

2.1 Fabrication of Al and Al-Ti Alloys

High purity granules of Al (99.9 wt.%) and Ti (99.99 wt.%) were used as the starting material for the fabrication of Al and its studied alloys as rods. ABB Germany Induction Melting Furnace was utilized to melt the charge amount in a graphite crucible at 200-kW under the protective Ar gas blown up through a graphite tube adjusted on the surface of the molten metal. Firstly, Al ingots were melted to above 660 °C, and then, different additions of Ti (0, 1, 2, 5, and 8 wt. %) were added into Al melt step by step. Following each Ti addition, the melt was heated to the point above a certain pouring temperature (900-1400 °C), depending on the amount of Ti added to Al to form the Al-Ti composites. To ensure that the reaction between Al and Ti particles completely occurred and that, consequently, Al-Ti intermetallic phase was formed, the mixture was kept at the above-mentioned temperature for about 15 min. Finally, each melted sample was poured into a worm cast iron mold (ϕ 12 × 160 mm) with a cooling rate of 150 °C/min, sand mold was used for cooling, and the temperature was recorded as a function of time using an Agilent 34970A multichannel electronic device. The alloys were fabricated in the laboratory of Central Metallurgical Research Institute (CMRDI), Helwan, Egypt.

XRD and SEM-EDAX tools were used to describe the composition and microstructure of the studied electrodes. It was found that the solid solution phase was formed, and the composition was homogeneous.

Table 1 Al-wt.%Ti compositions

Alloy No	Al	AT-1	AT-2	AT-3	AT-4
Composition	Al ₁₀₀ Ti ₀	Al _{98.7} Ti _{1.3}	Al _{98.27} Ti _{1.73}	Al _{94.7} Ti _{5.3}	Al _{91.27} Ti _{8.73}

2.2 Medium

0.5 M solution of both mentioned acids were prepared from Analytical grades of H₃PO₄ (85%) and HCl (37%) solutions using bidistilled water.

2.3 Surface Characterization

The prepared alloys in addition to Al were characterized utilizing x-ray diffraction thin film (X'Pert Pro, PANalytical, the Netherlands) consisting of a diffractometer with an iron filter and copper radiation was used with an accelerating voltage of 30 kV and a filament current of 20 mA and $\lambda=1.54$ Å. The morphology of each electrode surface was identified with the help of scanning electron microscopy (FE-SEM, QUANTA-FEG 250, the Netherlands) attached with EDX Unit (Energy Dispersive x-ray Analyses), with accelerating voltage 30 kV magnification 14x up to 1,000,000 and resolution for Gun.1n).

2.4 Microhardness Measurements

Vickers hardness was measured using a tester (LeizWetzlar, Ref Method ASTM E384:11a). Uncertainty measurements (\pm 95% confidence level) included humidity 31%, environmental temperature of 23 °C with a load of 100 g, and the dwell time of 10 s. The mean of the three measurements was taken to determine the hardness.

2.5 Density Functional Theory Calculations (DFT)

The effect of chemical structure variation of Al-Ti alloys on their electrochemical behavior was investigated through the DFT approach, using *B3LYP* with *LanL2DZ* basis set of theory (Ref 21, 22).

2.6 Electrochemical Measurements

The measurements were carried out on the disk electrodes (1 cm diameter) embedded in the holder of an Araldite. A series of emery papers (grade 200-1000-2000-4000) was used in polishing the surfaces of the working electrodes before each experiment until each surface became mirror-like smooth. Before inserting the working electrode in the electrochemical cell, each electrode surface was degreased in pure acetone and ethanol, and finally, it was washed using bidistilled water. The reference electrode, which was recognized for all potentials, was a saturated calomel electrode (SCE \approx 0.241 V), while the counter electrode was a wire of platinum. The two branches of cathodic and anodic Tafel lines were performed at a scan rate of 1 mV/s and the range of potential about \pm 250 mV concerning the potential of corrosion (E_{corr}). Each electrode was left for 30 min in the examined solutions (0.5 M HCl (pH \approx 0.35 \pm 0.1), and 0.5 M H₃PO₄ (pH \approx 1.30 \pm 0.1)) to reach the steady-state value (E_{corr}) prior to EIS measurements. The range of frequency was set from 100 kHz to 10 mHz with the potential amplitude of 10 mV in E_{corr} . All measurements were performed using VersaSTAT4potentiostat with Versastudio software; the data obtained from EIS measurements were fitted using ZSimpWin 3.6 software. A newly prepared solution and a collection of

clean surfaces were provided for each analysis. Experiments were carried out at different temperatures (25, 35, 45, and 55 ± 0.5 °C) for each studied surface in the investigated solutions, using the ultra-thermostat model Alpha RA8 for this purpose.

3. Results and Discussion

3.1 Chemical Composition of Samples

The composition of Al and Al-Ti alloys, as shown in Table 1, was analyzed using XRF analysis received from CMRDI (PANalyticalAxios Advanced XRF, Tokyo, Japan).

3.2 Microstructure of Al-Al₃Ti Composites in the Al-Ti System

Figure 1 shows the XRD pattern of the Al-wt.%Ti composites. In addition to the peaks of aluminum, only the peaks of Al₃Ti were found, indicating that only Al₃Ti phase was formed via an interaction between Al and Ti element during the process (Ref 4, 9). Table 2 shows the XRD analysis of Al-Al₃Ti composites with the addition of various amounts of Ti to Al. The size of Al₃Ti apparently increased with the increase of Ti content. The Ti particles were primarily distributed in aluminum grains, and as the content of Al₃Ti increased, the size of aluminum grains decreased (Ref 17). This means that the wet ability between Al₃Ti and the aluminum matrix was very strong and that the particles of Al₃Ti would serve as aluminum grain nucleation sites (Ref 9). Therefore,

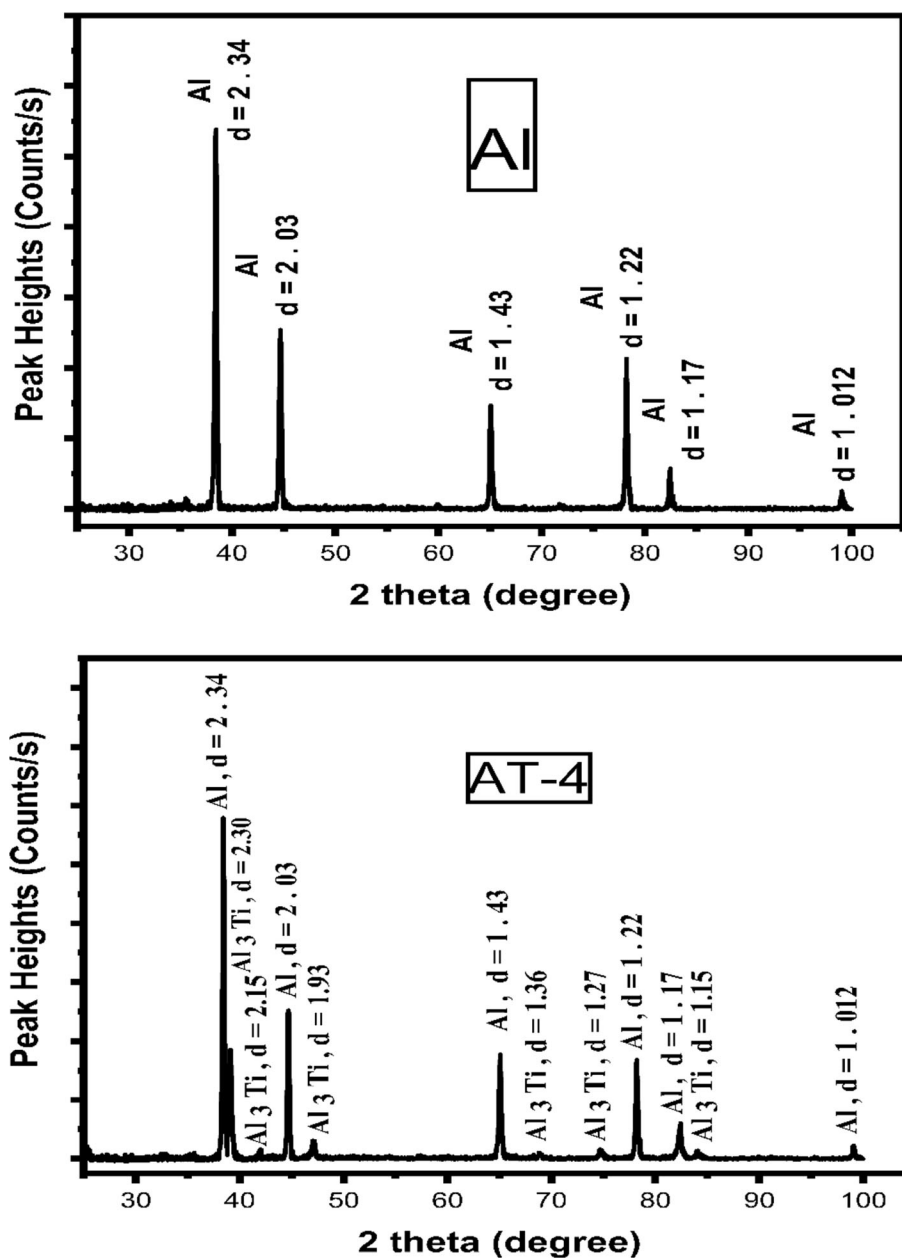


Fig.1 XRD pattern on the surface of prepared Al and AT-4 alloy

Table 2 Analysis of XRD

System	Phase designation	Crystal system	CrystalSize, nm
Al (Al ₁₀₀ Ti ₀)	Al	Cubic	52.61
AT-1(Al _{98.7} Ti _{1.3})	AlAl ₃ Ti	CubicTetragonal	51.9334.15
AT-2(Al _{98.27} Ti _{1.73})	AlAl ₃ Ti	CubicTetragonal	49.1539.11
AT-3(Al _{94.7} Ti _{5.3})	AlAl ₃ Ti	CubicTetragonal	41.2144.96
AT-4(Al _{91.27} Ti _{8.73})	AlAl ₃ Ti	CubicTetragonal	39.0350.27

higher interfacial bonding strength and thermal stability can be expected (Ref 19). The patterns for Al and the eutectic AT-4 alloy in Fig. 1 were compared; the pattern of higher Al peaks appeared at $2\theta=38.42, 44.65, 65.03, 78.20, 82.38,$ and 99.12 (JCPDS number: 00-004-0787), while the AT-4 pattern manifested that some Al particles seemed to be separated as the elemental phase (Cubic), interfering with the Al₃Ti matrix (Tetragonal) in the alloy sample. Besides, XRD revealed that higher intermetallic peaks of Al₃Ti particles were observed at $2\theta=39.08, 41.92, 44.69, 47.13, 74.74,$ and 82.42 (JCPDS number: 00-037-1449). The data also showed that Ti as a free element cannot be detected. This reveals that Ti content in the alloy is completely soluble in the Al matrix (Ref 23).

The crystal size was evaluated from the pattern of XRD by utilizing well-known Scherer's equation (Ref 23)

$$D_{hkl} = \frac{K\lambda}{\beta_{hkl}\cos\theta} \quad (\text{Eq 1})$$

where D_{hkl} was the size of crystal; λ was the wavelength (Cu $K_{\alpha}=1.54056$ Å); θ was the angle of reflection; K was the Scherer's somewhat arbitrary value that fell in the range from 0.87 to 1, and β_{hkl} was the full-width at half-maximum (FWHM). It was noticed that the grain size of composites was refined after adding a small amount of Ti, while the uniform distribution of Al₃Ti particles in the solid solution was retained. Table 2 shows the details of the XRD analysis.

3.3 Scanning Electron Microscopy (SEM)

Figure 2 shows the micrographs of SEM of the synthetic samples for Al and its investigated alloys. Many dark pores seem to be largely spread on the surface of pure Al (Fig. 2a). On the other hand, the addition of Ti amount to Al revealed the variation in the micrographs. It was observed that the dark pores significantly decreased with the small addition (5.3% Ti) of Ti to Al (Fig. 2b). Besides the regions of interdendritic compounds contained a solute segregated with dendritic lines. This indicated that the addition of 5.3% Ti had the ability to form an intermetallic compound of Al₃Ti. On the other hand, the dark pores on the surface seemed to have disappeared with the addition of 8.73% Ti, while more dendritic lines were spread on the surface compared to that with lower Ti content (5.3% Ti). This implied that the amount of the intermetallic compound of Al₃Ti increased due to an increase in the addition of Ti.

3.4 Mechanical Properties

Vickers microhardness test was utilized in measuring the values of hardness for both Al and Al-Ti composites. At least three measurements on each surface of the specimen were done, and the average of values was obtained for both Al and Al-Ti samples. The procedure of the Vicker microhardness test relied on Vickers pyramidal indenter with the Vickers hardness

number is given as $HV=0.185F/d^2$, where F was the applied load, and d was the average diagonal length in millimeters. The average values of microhardness for Al and Al-Ti samples were reported, as shown in Table 3. The increase in hardness was associated with the dispersion of the Al₃Ti intermetallic phase, as well as with the grain size of the matrix (Ref 24). This indicated that the formation of a precipitate of the intermetallic Al₃Ti particles, following the addition of Ti to Al, led to an increase in the hardness of the binary alloy(Ref 23, 25-28). The significant increase in microhardness in the case of AT-4 can be attributed to the formation of a large number of intermetallic compounds in the solid state (Ref 28). Intermetallic compounds are generally brittle and hard. ImageJ software was used to measure the porosity of aluminum and its alloys, which was calculated from SEM (Table 3). Such an influence of Ti added to Al resulted in a reduction of the grain size of Al accompanied by a lower amount and size of porosity and improved homogeneity of the pore distribution. Thus, one can conclude that adding Ti to Al significantly decreases its porosity.

3.5 Quantum Chemical Studies

The 3D model, charge distribution, and orbital occupation of the Al-Ti alloy were theoretically investigated through DFT calculation (Fig. 3).

Some global chemical descriptors, including *HOMO*, *LUMO*, energy gap, and others (Table 4), were used to estimate the chemical reactivity(Ref 29).

The structure–activity relationship (SAR) model was derived by correlating the practical activity (i_{corr}) of the under-study compounds with their calculated chemical descriptors (Table 4) (Ref 30). Theoretically derived SAR equations are formulated in Eq. (2 and 3).

$$i_{corr}(\text{at } 25^{\circ}\text{C in } 0.5\text{M H}_3\text{PO}_4) = 4.82 - 178.49E_{HOMO} - 52.28\omega \quad (\text{Eq 2})$$

$$i_{corr}(\text{at } 25^{\circ}\text{C in } 0.5\text{ M HCl}) = 1074.20 - 1031.31E_{HOMO} - 385.63\omega \quad (\text{Eq 3})$$

It is obvious from Eq. (2) and (3) that the practical activity depended on both HOMO energy (E_{HOMO}) and the electrophilicity index with different coefficients. The practical and calculated i_{corr} was compared, showing high agreement (Table 5).

3.6 Tafel Polarization Measurements

The curves in Fig. 4 compare the cathodic and anodic polarization (Tafel plots) between Al and AT-3 alloy (Fig. 4a), as well as Al and AT-4 alloy (Fig. 4b) in 0.5 M solution of HCl at 25 °C. The data exhibited the polarization curve of the cathodic branch that shifted toward higher current densities with the addition of both 5.3 and 8.37% Ti to Al. Such a shift resulted from the reaction of hydrogen evolution on the surface

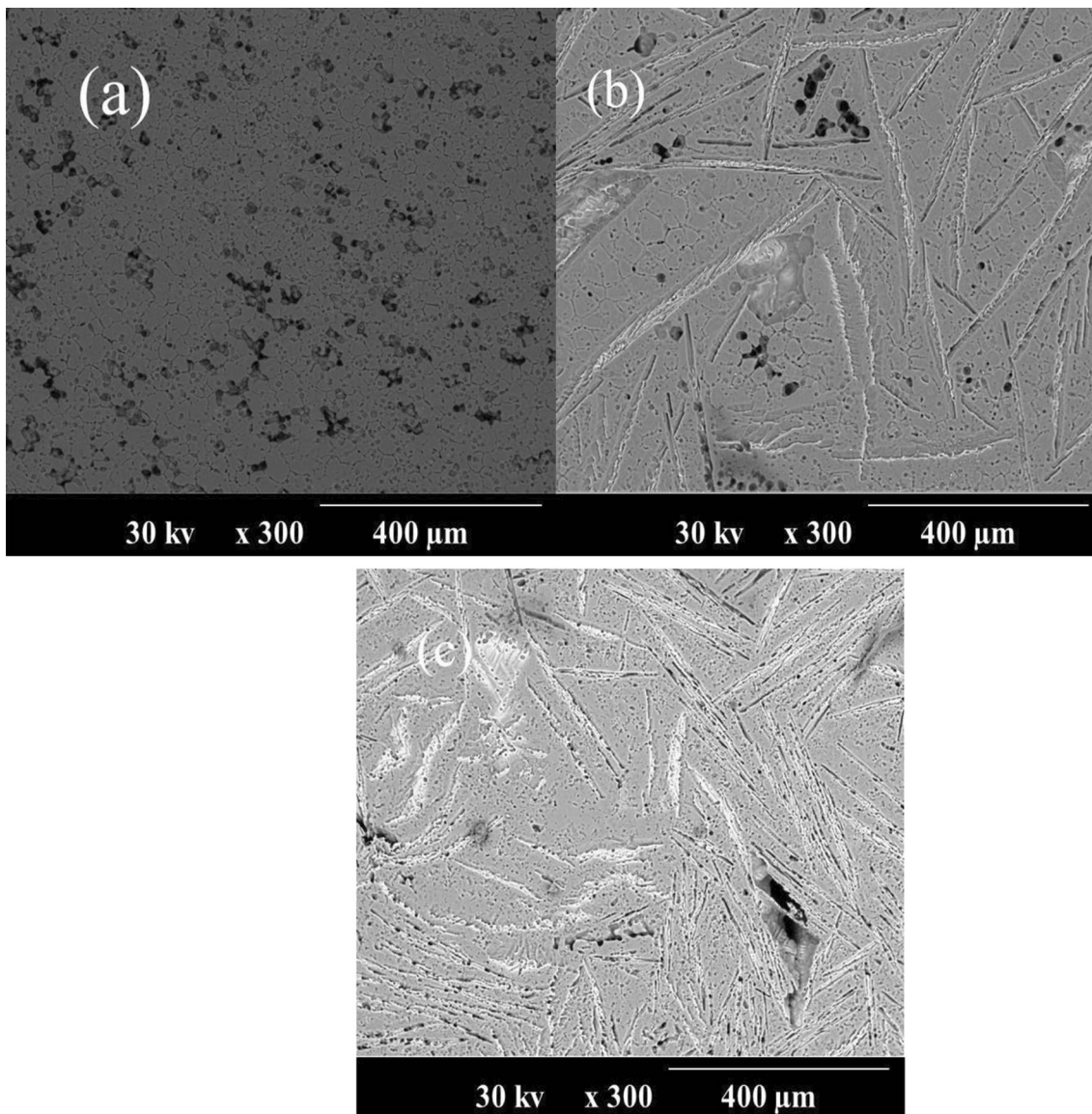


Fig. 2 Photographs of SEM of some studied surfaces for samples (a) Al, (b) AT-3, and (c) AT-4 magnified at 300 times

Table 3 Microhardness and porosity% studies of Al and Al-Ti alloys

Alloy No	Composition	Microhardness, HV	Porosity, %
Al	$Al_{100}Ti_0$	20 ± 0.1	25.6 ± 1.9
AT-1	$Al_{98.7}Ti_{1.3}$	24.8 ± 0.4	22.3 ± 1.2
AT-2	$Al_{98.27}Ti_{1.73}$	25 ± 0.42	19.3 ± 1.6
AT-3	$Al_{94.7}Ti_{5.3}$	27.4 ± 0.1	15.71 ± 2.1
AT-4	$Al_{91.27}Ti_{8.73}$	37.4 ± 0.7	9.35 ± 1.6

of the alloy, which was higher than that of Al. The latter was presumably induced by the action of Al_3Ti particles on the alloy surface detected with x-ray diffraction. The above action, in its turn, could be ascribed to the hydrogen over-potential on the Al_3Ti particles, which was lower than that on the Al surface (Ref 28). Consequently, the presence of Al_3Ti particles on the surface facilitated the reaction of hydrogen evolution. The branch of the anodic process shifted to lower densities of current in the two mentioned alloys. It revealed that the rate of current change with potential variation was lower during

polarization of the anodic process than that of polarization of the cathodic one (Ref 31). This behavior also showed that Al_3Ti particles on the alloy surface played an important role in covering the anodic sites and enhancing the anodic corrosion resistance, which reduced the dissolution of Al (Ref 32). The value of E_{corr} shifted toward a more positive direction after adding Ti to Al. This indicated that the decrease in the anodic current branch (Tafel plots) and a shift to a more positive direction in E_{corr} as a result of Ti alloying with Al could be attributed to the suppression of some active sites on the anodic

alloy surface. This means that the changing rate of current density with the variation of potential was smaller during the process of anodic polarization compared to that of the cathodic process (Ref 33). However, the total i_{corr} of anodic and cathodic branches extrapolation revealed that i_{corr} value was higher for Al-Ti alloy than that for Al. Hence, the cathodic current value was higher and more predominant than that of the anodic one due to the depolarization action of the Al_3Ti phase on the cathodic site (Ref 34).

The porosity (P_R) of Al and its alloys (after corrosion) was evaluated utilizing polarization resistance (R_p), which is determined from potentiodynamic polarization curves according to the following equations (Ref 35):

$$R_p = \frac{B}{i_{corr.}} \text{ and } B = \frac{b_a b_c}{2.303(b_a + b_c)} \quad (\text{Eq 4})$$

Figure 5 exhibits the variation of porosity percent with Ti content alloying with Al at 25 °C. It is noticed that the porosity percent (P_R) increases with increasing Ti content in the alloy in both HCl and H_3PO_4 . This indicates that the corrosion resistance decreases with increasing Ti content. Accordingly, the variation in porosity as a result of Ti alloying with Al is

confirmed by the obtained results from potentiodynamic polarization curves and impedance spectra data. The total porosity, which may be determined from the polarization resistance, is defined hereafter(Ref 36, 37).

$$P_R = \frac{R_p^o}{R_p} \times 100\% \quad (\text{Eq 5})$$

where P_R , R_p^o and R_p correspond to the total porosity, polarization resistance of the unalloyed and alloyed aluminum with titanium, respectively.

3.7 The Effect of Temperature

The effect of varied temperature on the cathodic and anodic polarization curves of Al and AT-4 alloy in 0.5 M solution of HCl in the range from 298 to 328 K (25-55 °C) and with the rate of a scan of 1 mV/s was studied. It was found that the branches of cathodic and anodic polarization lines had no significant influence on their general shape after varying temperatures. However, as the temperature grew, the two branches of anodic and cathodic processes shifted to higher current densities. The temperature became more effective as a

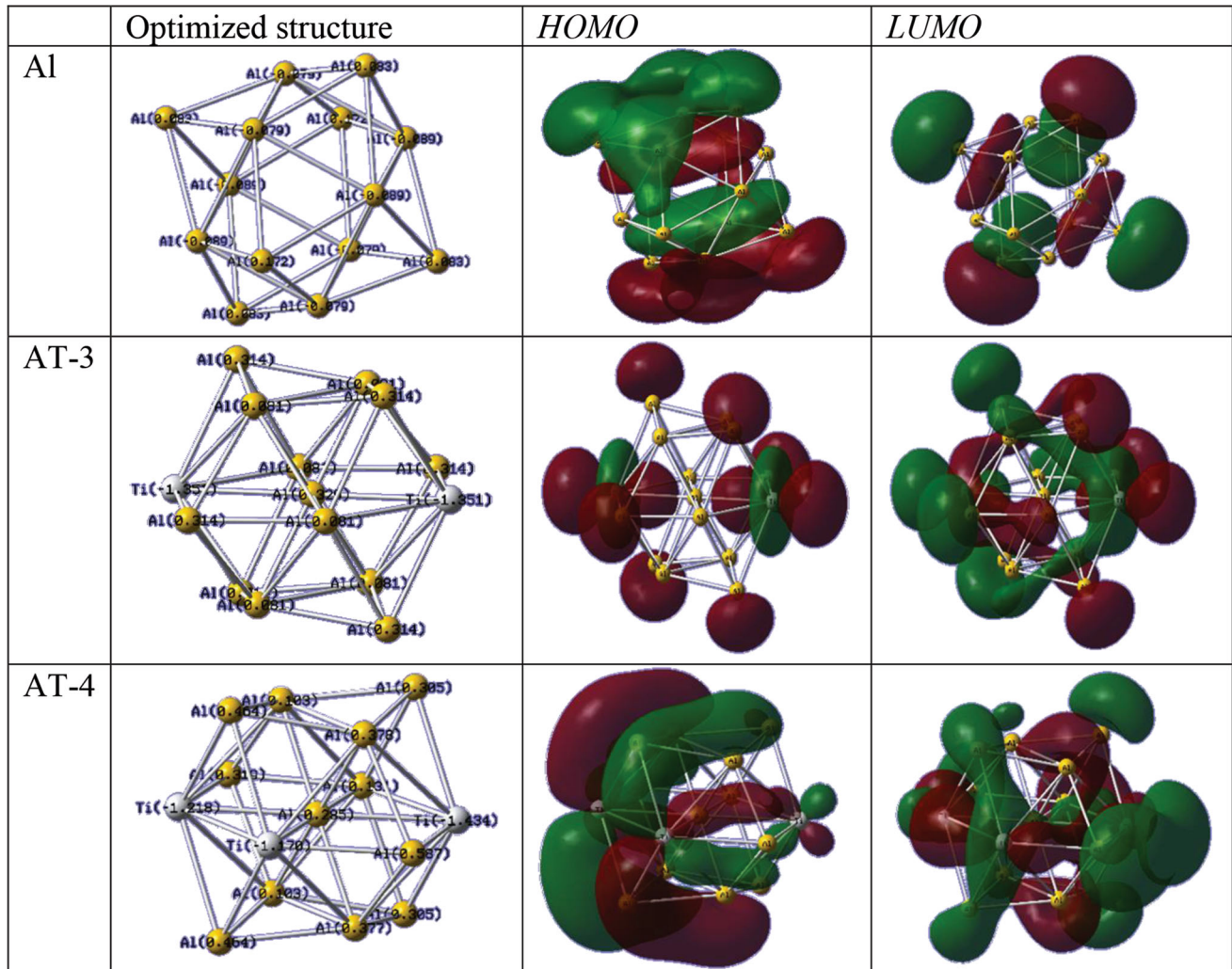


Fig. 3 Comparison of electronic structures of the optimized structure between the native Al and Al-Ti (AT-3 and AT-4) alloy calculated using DFT/LanL2dz method

Table 4 Calculated HOMO, LUMO, energy gap (ΔE), electronegativity (χ), chemical hardness (η), softness (σ), chemical potentials (μ), electrophilicity index (ω), and nucleophilicity (Nu), by eV unit of the native Al and Al-Ti (5.3, and 8.73%) alloys

Samples	E_{HOMO}	E_{LUMO}	ΔE	χ	μ	η	σ	ω	Nu
Al	-5.12	-3.85	1.26	4.48	-4.48	0.63	0.79	15.90	0.06
AT-3	-4.26	-3.10	1.17	3.68	-3.68	0.58	0.86	11.58	0.09
AT-4	-4.12	-3.01	1.11	3.57	-3.57	0.55	0.90	11.48	0.09

Table 5 Practical and calculated i_{corr} by SAR model based on the DFT approach at 25 °C in 0.5 M H_3PO_4 , and 0.5 M HCl of the native Al and Al-Ti (5.3, and 8.73%) alloy

Samples	0.5 M H_3PO_4 , 25 °C		0.5 M HCl, 25 °C	
	i_{corr} (practical)	i_{corr} (calculated)	i_{corr} (practical)	i_{corr} (calculated)
Al	87.42	87.44	223.00	222.99
AT-3	159.77	159.79	1001.99	1001.99
AT-4	140.01	140.02	896.17	896.16

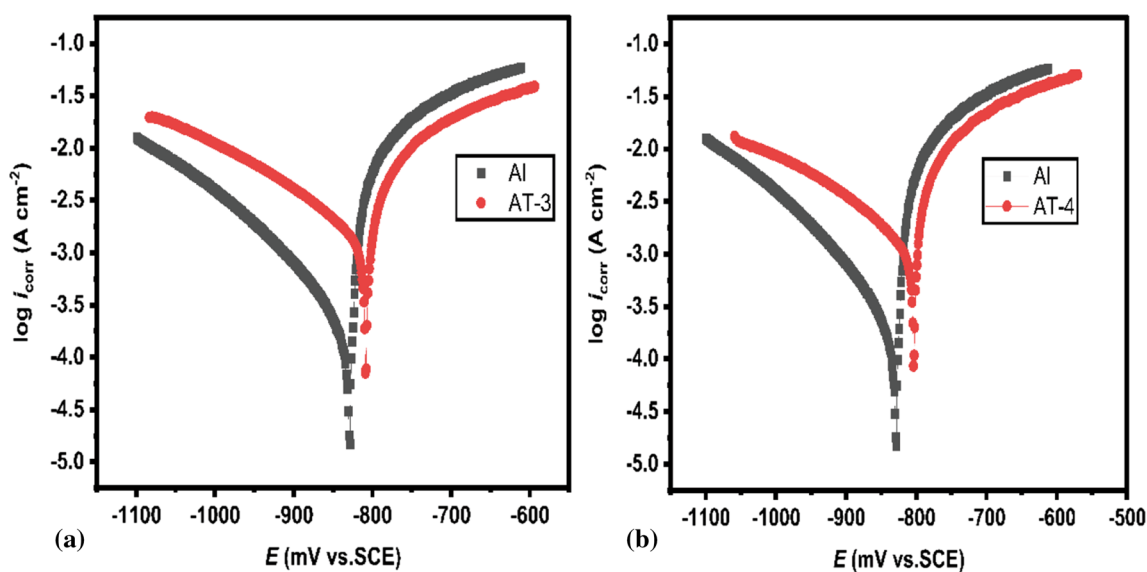


Fig. 4 Polarization curves for Al with AT-3 alloy (a) and Al with AT-4 alloy (b) in 0.5 M solution of HCl at 298 K (25 °C) and a rate of scan = 1 mV/s

result of an increase in the titanium content in the alloy. On the other hand, the rate of current densities of both branches increased at higher temperatures of AT-4 electrode compared to that of aluminum. It was explained by the fact that titanium alloying with aluminum improved the processes of cathodic and anodic reaction with a temperature increase due to the formation of rich particles from solid titanium composite on the surface.

Table 6 shows the electrochemical parameters of Al and its investigated alloys at different temperatures. These parameters include E_{corr} , i_{corr} , as well as the slopes of Tafel b_c and b_a of cathodic and anodic processes, respectively, for the studied electrodes in 0.5 M solution of HCl. The data showed that i_{corr} increased with raising the temperature of both Al and its studied alloys. On other hand, i_{corr} gradually increased with the raised amount of Ti in the specimen up to 5.3%Ti (AT-3). That phenomenon could be ascribed to the formation of more active sites on the surface of alloy electrodes after incremental adding

Ti to Al; hence, it was concluded that the number of active sites gradually increased with an increase in Ti content in the alloy. In other words, the presence of the Al_3Ti phase on the surface of the alloy leads to the formation of weak sites in the thin oxide layer; consequently, the corrosion processes were initiated. Accordingly, the attack of active sites on the alloy surface by Cl^- ions is easier, resulting in depolarization action (Ref 38). In other words, the formation of higher active sites means an increase in anodic to cathodic area ratio (Ref 23). Consequently, the surfaces expose more weakly bonded sites, leading to a higher rate of dissolution, particularly in corrosive solutions. However, at higher Ti content in the alloy (AT-4), the i_{corr} relatively decreased compared to that of alloy AT-3 due to higher amounts of Al_3Ti particles formed on the surface, resulting in a less heterogeneous surface (Ref 28). The values of b_c and b_a (Tafel slopes) in Table 6 revealed higher values of b_c than those of b_a ones. That was an indication that the values of cathodic exchange current density were lower than those of

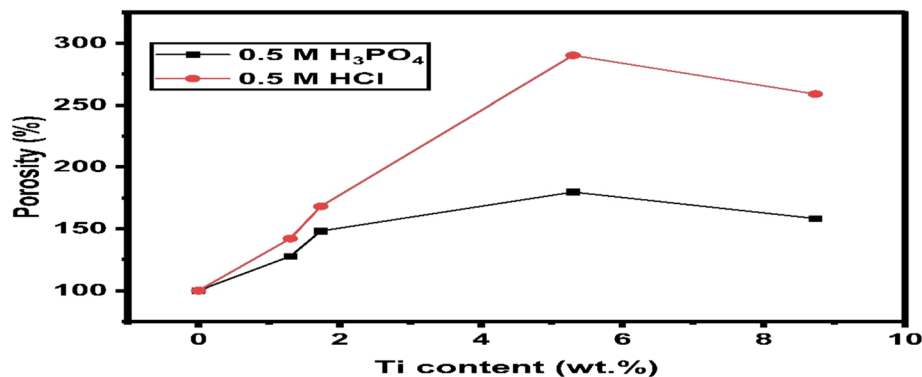


Fig. 5 Plots of the porosity as a function of Ti content (wt.%) in 0.5 M HCl and H₃PO₄ at 25 °C

anodic counterparts. Therefore, one could conjecture that the overall corrosion kinetics were under cathodic control (Ref 39) of all investigated electrodes in a 0.5 M solution of HCl.

3.8 Electrochemical Behavior of Al and its Investigated Alloys in a Solution of H₃PO₄

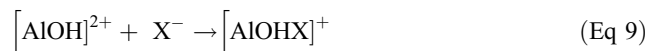
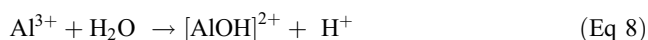
The polarization curves of pure Al with both alloy AT-3 and AT-4 specimens are represented in Fig. 6a and b. The obtained data revealed two branches of both the reaction of hydrogen evolution and the anodic dissolution process, which clearly moved to higher densities of current after adding Ti to Al. Also, the potential of corrosion (E_{corr}) shifted to more positive values with Ti addition to Al. Based on these observations, it can be concluded that Al₃Ti particles on the surface of the alloy electrode had a depolarizing action (Ref 28). Therefore, the active sites on the surface of the alloy electrode occurred as a result of the founding phase of Al₃Ti.

The corrosion parameters were precisely estimated, depending on the lines slope of cathodic and anodic polarization curves. The i_{corr} values for the studied electrodes were evaluated by extrapolating the cathodic and anodic lines of the polarization to E_{corr} . The b_c in Table 7 exhibits lower values (98-101 mVdec⁻¹) compared to the theoretical ones. This behavior can be attributed to the soluble species formed on the electrode surface, in addition to a very thin film on the surface formed in H₃PO₄ than that in HCl solution. It indicated that the cathodic reaction of Al and its investigated alloys in the H₃PO₄ solution were controlled by the charge transfer. Besides, the anodic Tafel slope (b_a) values were high (137-142 mVdec⁻¹), which contradicted those observed in the HCl solution (20-30 mVdec⁻¹). This observation (in H₃PO₄) can be explained given the corrosion products diffusion, which was formed on the active sites of anodic parts by the polarization of concentration (Ref 40).

From the results displayed in Table 6 and 7, it is evident that the rate of corrosion was higher in HCl than that in H₃PO₄. Moreover, the corrosion resistance of the AT-3 alloy was lower than that of the AT-4 alloy, while AT-4 had a higher Ti content than AT-3. This may have resulted from changes in the growth mode and the formation of Al₃Ti phase particles. The latter may be caused by the changes in Al₃Ti morphology that made the planes of crystals braided to the surrounding particles, inducing grain size refining (Ref 41, 42). Besides, Ti addition to Al leads to the formation of Al₃Ti particles, and thus, the corrosion resistance of the mentioned alloys decreased, which contra-

dicted the results reported by Sequeira and Das (Ref 43, 44). This is explained by the formation of Al₃Ti particles as a result of Ti alloying with Al; therefore, a certain potential difference between the platelets of Al₃Ti and Al matrix occurred (Ref 45). Accordingly, the Ti addition caused an increase in the number of galvanic cells. Thus, the corrosion resistance of the mentioned alloying composites decreased compared to that reported for the Al matrix.

The rate of corrosion gradually increased with a temperature rise, indicating that the thin oxide film found on the electrode surface dissolved rapidly; consequently, the rate of corrosion process was enhanced. The mentioned trend could be attributed to enhancement in the dissolution of the chemical film due to the presence of chloride, phosphate ions, and $Al(OH)_4^-$ between the film surface and the interface of the solution. As a consequence of the breakdown of the film by the electrolyte, the film of passive became very thin, more porous, and non-protective with the temperature rise (Ref 46). It was also noted that with the rising temperature, the b_c and b_a slopes of Tafel plots remained almost constant. That suggested that the temperature only simulated the corrosion surface without influencing the corrosion mechanism (Ref 47). The process of corrosion of the investigated electrodes could be described as formation of an oxide layer in the air, which initially turned into the thickness, leading to formation of the hydrated crystalline alumina when exposed to an aqueous solution (Ref 45). The anodic corrosion phase in acidic solutions was the metal dissolving (Ref 48) from the electrode surface into an electrolyte as follows:



The principal process of cathodic reaction was the reduction of hydrogen ions to produce gas of hydrogen.



Table 6 Tafel polarization studies of Al and Al-Ti specimen in 0.5 M solution of HCl

Samples	Temp., °C	$-E_{\text{corr}}$, mV vs. SCE	i_{corr} , $\mu\text{A}\cdot\text{cm}^{-2}$	b_a , $\text{mV}\cdot\text{dec}^{-1}$	$-b_c$, $\text{mV}\cdot\text{dec}^{-1}$
Al	25	832.6	223	19.4	122.3
	35	794.9	421.3	33.4	131
	45	809.8	765.2	34.7	132.8
	55	881	1444	23.5	121
AT-1	25	822.04	400.82	25.40	127.60
	35	870.11	759.18	24.30	125.80
	45	851.68	1119.53	25.00	126.60
	55	804.48	1523.34	31.80	127.90
AT-2	25	822.16	503.84	22.70	120.10
	35	819.98	1013.74	23.20	125.40
	45	808.86	1316.84	29.70	120.30
	55	850.76	2055.12	29.00	129.00
AT-3	25	808.65	1001.99	32.20	133.10
	35	811.42	1495.41	31.10	129.90
	45	841.58	2000.00	25.90	120.60
	55	853.19	3012.03	35.20	119.20
AT-4	25	804.36	896.17	32.50	129.80
	35	804.63	1327.99	27.40	123.10
	45	863.43	1854.35	29.60	119.60
	55	823.12	2544.62	32.40	120.00

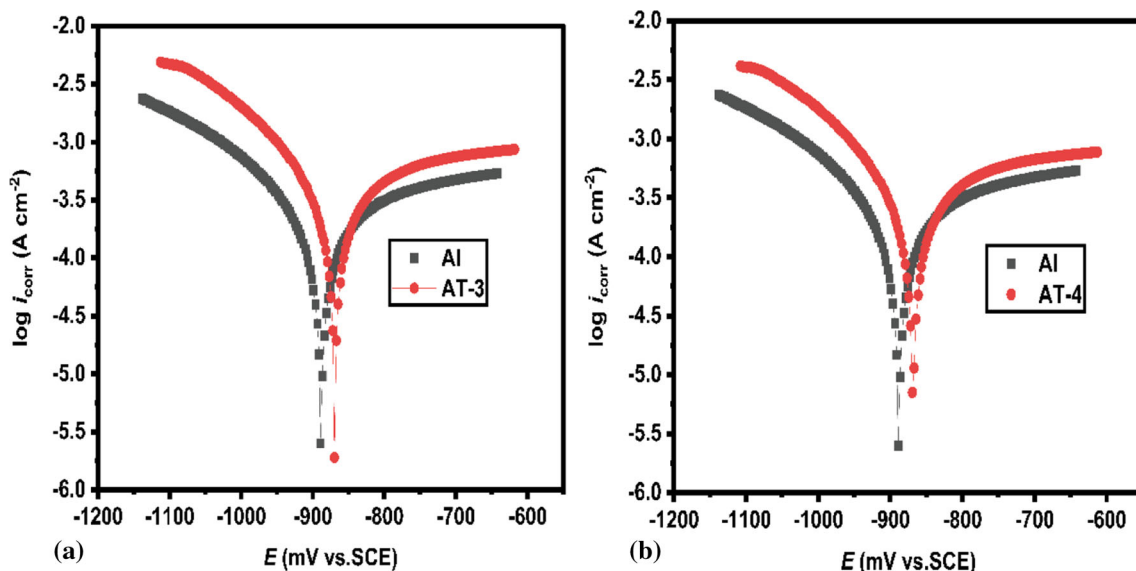


Fig. 6 Polarization curves of Al with AT-3 alloy (a) and Al with AT-4 alloy (b) in 0.5 M solution of H_3PO_4 at 298 K (25 °C) and at a rate of scan=1 mV/s

3.9 Thermodynamic Parameters Measurements

Figure 7 a and b shows the plots of Arrhenius for the studied electrodes in the investigated acids solutions. The energy of activation values was evaluated using the equation of Arrhenius (Ref 49).

$$\log i_{\text{corr}} = \log A - \frac{E_a}{2.303RT} \quad (\text{Eq 12})$$

where the absolute temperature was T , the constant was A , the universal gas constant was R , and the energy of activation was E_a . The slope of $\log i_{\text{corr}}$ vs. $1/T$ was determined. E_a values of the investigated electrodes in both HCl and H_3PO_4 were evaluated from these slopes and given in Table 8.

The curves in Fig. 8 refer to the $\log (i_{\text{corr}}/T)$ vs. $1/T$ for aluminum and its investigated alloys after 30 min immersion in the studied acids. The data in this figure showed different

straight lines with various slopes of $(-\Delta H/2.303R)$; two different intercepts of the $\log R/Nh + \Delta S/2.303R$ were evaluated with the help of the following equation (Eyring Equation) (Ref 50, 51):

$$i_{\text{corr}} = RT/Nh \exp(\Delta S/R) \exp(-\Delta H/RT) \quad (\text{Eq 13})$$

where Planck's constant was h , Avogadro's number was N , the enthalpy of activation was ΔH , and the entropy of activation was ΔS . The values evaluated for (E_a) , (ΔH) , and (ΔS) of the investigated Al and Al-Ti alloys in 0.5 M solution for both HCl and H_3PO_4 are listed in Table 8.

As shown in Table 8, the value of activation energy (E_a) was higher than 20 kJ mol^{-1} for the investigated electrodes. This revealed that the processes of corrosion were under reaction control by the surface (Ref 52-54). It was evident that the activation energy decreased as a result of Ti alloying with Al in

Table 7 Tafel polarization studies of Al and Al-Ti alloys in 0.5 M H₃PO₄

Samples	Temp., °C	-E _{corr} , E vs. SCE	i _{corr} , μA.cm ⁻²	b _a , mV.dec ⁻¹	-b _c , mV.dec ⁻¹
Al	25	888.42	87.42	137.40	98.60
	35	862.58	165.09	138.40	101.00
	45	845.37	312.76	141.10	101.90
	55	845.32	527.07	139.20	100.20
AT-1	25	853.92	112.36	138.40	99.20
	35	851.79	188.38	139.20	99.40
	45	829.37	386.13	138.80	99.00
	55	843.42	583.49	139.50	100.70
AT-2	25	881.25	128.73	137.20	97.70
	35	836.26	211.86	138.90	98.10
	45	839.35	402.62	142.80	99.10
	55	838.23	686.69	138.90	101.00
AT-3	25	865.61	159.77	138.00	101.20
	35	850.39	299.17	139.90	99.60
	45	853.93	453.96	138.50	101.80
	55	831.23	788.98	141.80	99.90
AT-4	25	865.80	140.01	138.30	100.20
	35	869.02	252.18	140.10	99.10
	45	849.55	442.62	141.80	99.70
	55	839.35	730.83	140.50	100.40

the two mentioned acids. Moreover, there was a considerable decrease in the activation energy in the case of the hydrochloric acid, which was not observed for the phosphoric acid. That could be interpreted as an increase in corrosion processes in HCl in comparison to the former in the phosphoric acid. On the other hand, it was noticed that ΔS was high and negative, suggesting that the process of association was higher than that of dissolution in the rate-determining process due to the presence of activated complex (Ref 55). This indicated that the reactant moved to the activated complex, which resulted in the disorder decrease. The ΔS value increased, while an increase in Ti content in both acids implied that dissolution of Al and Al-wt.%Ti alloys was facilitated since the content of the Al₃Ti phase increased. The decrease in ΔH with an increase of Ti content in the investigated alloy electrodes manifested that the dissolution of Al was fast. The positive values of ΔH testified for the corrosion reaction in an endothermic process (Ref 56).

3.10 Electrochemical Impedance Spectroscopy (EIS) Measurements

The measurements of EIS of the investigated electrodes in 0.5 M for both HCl and H₃PO₄ were examined to support the data obtained from potentiodynamic polarization. EIS results are tabulated in Table 9 and 10, respectively, for 25 °C. To better understand the interface reaction between Al-based alloys and the electrolytic solution for both Cl⁻ and PO₄³⁻ ions, EIS measurements were performed and compared. The curves of a and b in Fig. 9 and 10 show the plots of Nyquist and Bode-phase, respectively, for the studied electrodes in 0.5 M for both HCl and H₃PO₄ at E_{corr}. These plots revealed semicircles, evident that the electrochemical processes were mainly charge transfer controlled. Figure 9a presents the data for the experiment under high-frequency conditions where a loop of capacitive was observed, which was ascribed to the formation of an oxide layer on the surface of the Al electrode. Bessone et al. (Ref 57) and Brett (Ref 58) reported similar behavior. This implies that the surface was covered with a layer of oxide during pretreatment in the examined solution of the studied electrodes before each experiment, because the Al surface very easily reacted with oxygen to form the passive film (Ref 59). It

could be associated with the surface of the layer's dielectric properties (Ref 60). Yet, at low frequency, the origin of the large inductive loop was still unknown. It could be assumed that such behavior was caused by the ion movement on the electrode surface due to the physical processes (Ref 12). This expectation can be more pronounced when the adsorption of charged intermediates can be included in an inductive loop. It is expected that OH⁻ or O²⁻ ions are formed at the metal/oxide interface.

Relaxation of adsorbed species, like H_{ads}⁺, was suggested by Lenderink et al. (Ref 61). Adsorption of Cl⁻ (Ref 62) and the ion of oxygen (Ref 63) or the species of inhibitor (Ref 64) on the surface of electrode were additionally suggested for relaxation of adsorbed intermediates. The re-dissolution of the oxide layer on the surface (Ref 65) or dissolving Al (Ref 62) at low frequencies might also be due to adsorbed oxygen ions. Inductive behavior of the pitted active state was also observed and ascribed to modulation of the surface area or the property of the salt film modulation (Ref 66).

Cinderey and Burstein (Ref 59) reported that producing a free-from-an-oxide Al surface was rather challenging, even though the surface was prepared by using a freshly produced method, given its ability to very quickly oxidate by oxygen. It should be noted that Al₂O₃ could be significantly dissolved in the H₃PO₄. The first capacitive loop at HF would therefore be relevant to the dissolving mechanism of the Al/Al₂O₃/solution interface (Ref 58). At first, Al⁺ species were formed at the inner interface of Al/Al₂O₃ during that process, and when they migrated via the Al₂O₃/electrolyte interface they could further be oxidized to Al³⁺. The data showed that the semicircles seemed to be not ideal, confirming that there was a dispersion of frequency, resulting from the roughness and inhomogeneity of the electrode surface (Ref 67, 68). The adsorption-desorption process of the formed intermediates on the Al surface leads to the appearance of a small inductive loop at MF (Ref 69). Intermediates were thought to contain H_{ads}⁺ (Ref 70), and acid anions (PO₄³⁻, H₂PO₄⁻, HPO₄²⁻) on the aluminum electrode surface. The second loop of capacitive at low frequency could be attributed to Al-dissolution (Ref 71). The process of relaxation at LF was formed due to incorporation with adsorption of PO₄³⁻ ions through the film of oxide.

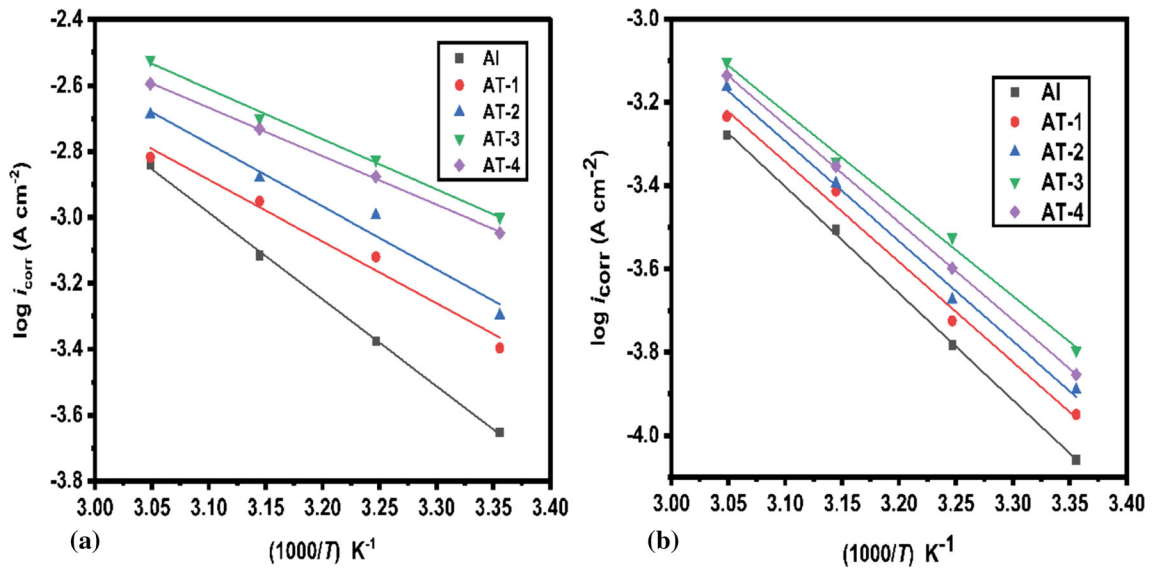


Fig. 7 Arrhenius plots collected after 30 min immersion in 0.5 M solution of both two acids (a) HCl and (b) H₃PO₄ for Al and Al-Ti alloys over the temperature range of 25-55 °C

Table 8 Thermodynamic parameters of the corrosion process of Al and Al-Ti specimens in 0.5 M solution for both H₃PO₄ and HCl after 30 min of immersion

Samples	Activation parameters					
	0.5 M H ₃ PO ₄			0.5 M HCl		
	E_a , kJ.mol ⁻¹	$-\Delta S$, J.mol ⁻¹ .K ⁻¹	ΔH , kJ.mol ⁻¹	E_a , kJ.mol ⁻¹	$-\Delta S$, J.mol ⁻¹ .K ⁻¹	ΔH , kJ.mol ⁻¹
Al	49.03	166.82	46.43	50.36	154.71	47.76
AT-1	46.02	174.99	43.43	36.52	197.74	33.27
AT-2	45.99	174.14	43.39	35.86	193.61	33.92
AT-3	42.35	184.10	39.75	29.18	213.19	26.58
AT-4	44.88	176.82	42.28	28.18	217.36	25.59

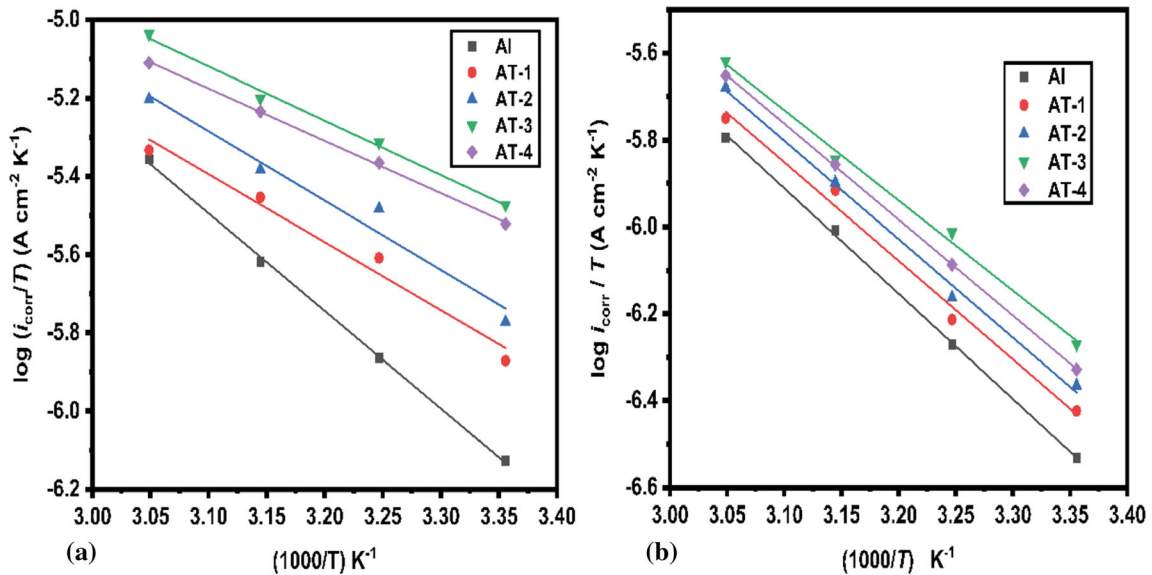


Fig. 8 $\log(i_{corr}/T)$ vs. $1/T$ plots collected after 30 min immersion in 0.5 M solution of two acids: (a) HCl and (b) H₃PO₄ of Al and Al-Ti alloys over the temperature range of (25-55 °C)

Table 9 EIS studies of Al and Al-Ti alloys in 0.5 M HCl at 25 °C

Samples	$R_1, \Omega \cdot \text{cm}^2$	$CPE(Q), \mu\text{F} \cdot \text{cm}^{-2}$	n	$R_2, \Omega \cdot \text{cm}^2$	$L_3, \text{H} \cdot \text{cm}^2$	$R_3, \Omega \cdot \text{cm}^2$
Al	5.119	59.490	0.926	95.410	73.440	14.150
AT-1	4.088	107.500	0.896	80.690	47.890	43.920
AT-2	3.590	69.530	0.969	54.880	38.090	11.180
AT-3	4.526	235.100	0.890	26.210	10.570	3.275
AT-4	4.936	322.700	0.862	39.840	45.660	13.390

Table 10 EIS studies of Al and Al-Ti alloys in 0.5 M H₃PO₄ at 25 °C

Samples	$R_1, \Omega \cdot \text{cm}^2$	$CPE(Q), \mu\text{F} \cdot \text{cm}^{-2}$	n	$R_2, \Omega \cdot \text{cm}^2$	$C_2, \mu\text{F} \cdot \text{cm}^{-2}$	$R_3, \Omega \cdot \text{cm}^2$	$L_4, \text{H} \cdot \text{cm}^2$	$R_4, \Omega \cdot \text{cm}^2$	$C_5, \text{mF} \cdot \text{cm}^{-2}$	$R_5, \Omega \cdot \text{cm}^2$	$R_p, \Omega \cdot \text{cm}^2$
Al	17.770	18.438	0.888	50.193	9.354	66.627	0.882	12.016	44.732	63.224	192.060
AT-1	18.230	40.097	0.870	45.733	9.137	67.423	0.842	10.021	53.080	53.107	176.285
AT-2	12.330	54.913	0.860	34.349	9.856	76.052	0.758	10.328	58.610	51.448	172.176
AT-3	11.910	226.000	0.817	11.950	28.597	66.510	0.405	5.002	139.600	22.517	105.979
AT-4	18.005	128.192	0.849	47.567	29.526	36.530	0.512	6.364	89.125	33.447	123.907

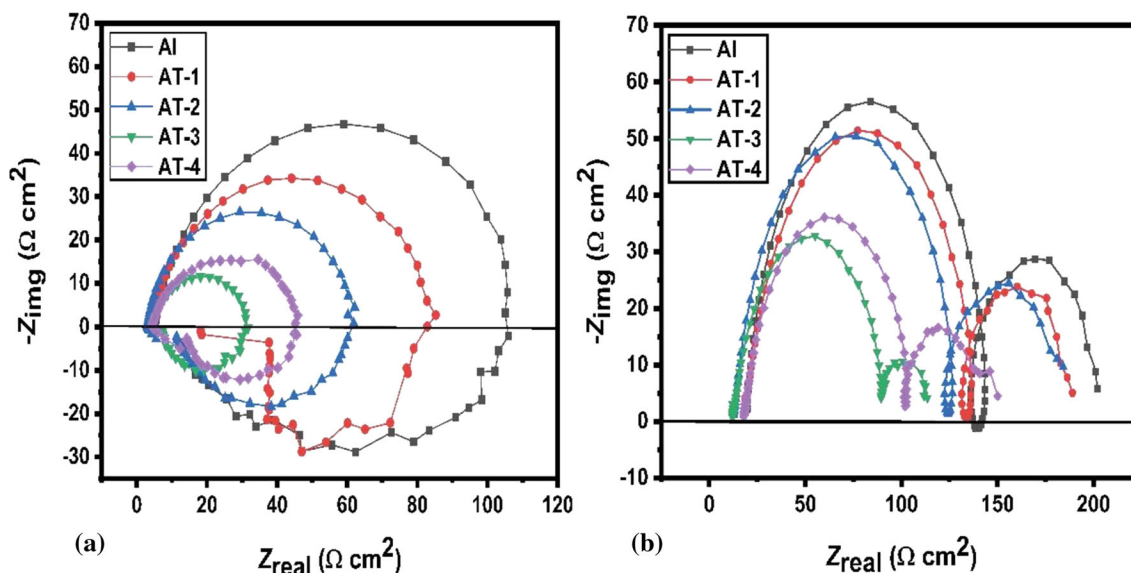


Fig. 9 Nyquist plots collected after immersion of the two studied acids in 0.5 M for 30 min: (a) HCl and (b) H₃PO₄ for Al and Al-Ti alloys

The impedance parameters of Fig. 11b, which were defined from the equivalent circuit, could be suggested, namely: resistance of solution (R_1), the resistance of charge transfer (R_2), the resistance of inductive (R_4), inductance (L_4), element of constant phase (CPE) (Q_1), and resistances R_3 , R_4 and R_5 , which corresponded to the first loop of capacitive at HF, the inductive loop at MF, and the second loop of capacitive at LF, respectively (Ref 72), as well as C_1 and C_2 capacitors. The resistance of polarization (R_p) and the twofold layer capacitance (C_{dl}) are evaluated with Eq. 14 and 15 (Ref 73):

$$R_p = R_2 + R_3 + R_4 + R_5 \quad (\text{Eq 14})$$

$$c_{dl} = c_1 + c_2 \quad (\text{Eq 15})$$

The CPE was used in place of a capacitor to compensate for deviations from the ideal dielectric behavior arising from the

nature of the inhomogeneous surfaces. The element of constant phase (Q) had the following definition (Ref 74):

$$Q = Y_0^{-1} (j\omega)^{-n} \quad (\text{Eq 16})$$

where Y_0 was the proportional factor, and ω was the angular frequency in rad s^{-1} ($\omega = 2\pi f_{\text{max}}$). The deviation parameter was n ($-1 \leq n \leq +1$), which corresponded to the phase shift. If $n=0$, Q represented a pure resistor, for $n=-1$ an inductor; and for $n=+1$ a pure capacitor; $j=(-1)^{1/2}$ was an imaginary number. The parameter of double electric capacitance was C_{dl} with the following equation:

$$C_{dl} = Y_0 (f_{\text{max}})^{n-1} \quad (\text{Eq 17})$$

where f_{max} was the maximum frequency related to the maximum impedance in the Nyquist plot. Finally, the obtained results from EIS measurements showcased a similar behavior to that in the potentiodynamic polarization experiments.

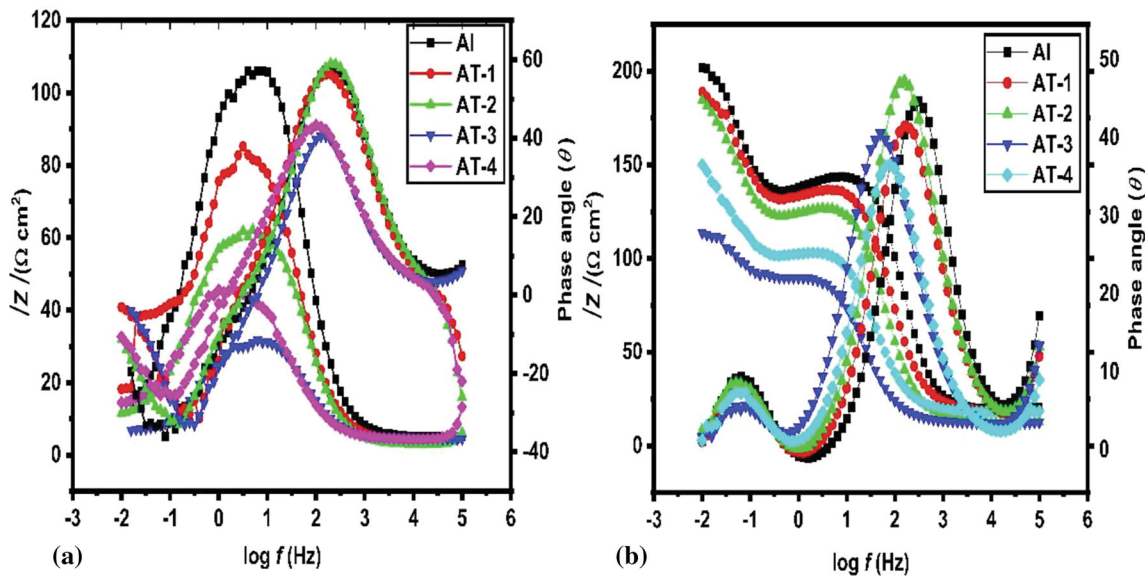


Fig. 10 Bode and phase plots collected after immersion of the two studied acids in 0.5 M for 30 min: (a) HCl and (b) H₃PO₄ for Al and Al-Ti alloys

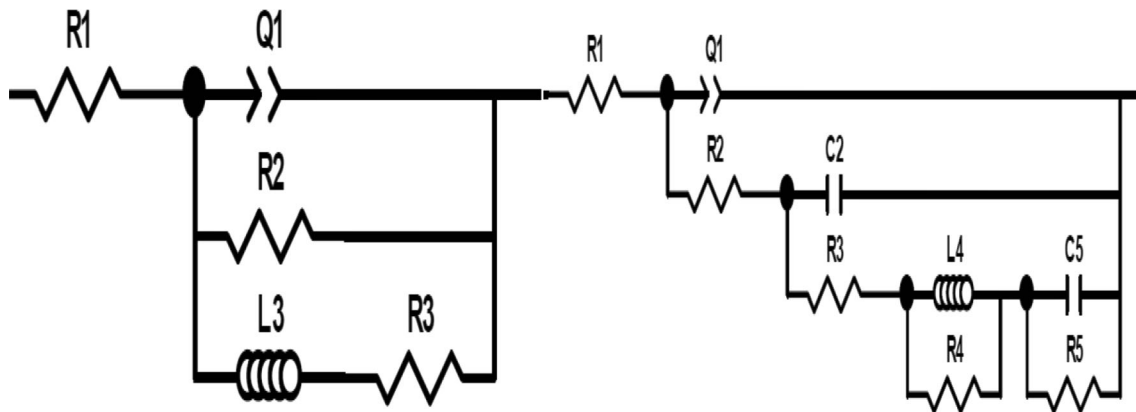


Fig. 11 The model used of equivalent-circuit for the experimental fitting of EIS results for Al and Al-Ti alloys in 0.5 M of the two studied acids: (a) HCl and (b) H₃PO₄

3.11 Microscopic Tests of Al and its Alloys (SEM)

Figure 12 shows SEM photographs of Al, AT-3, and AT-4 alloys after potentiodynamic polarization tests in the examined HCl solution. The image in Fig. 12a reveals that the Al surface seemed to be completely covered with a white layer (Al(OH)₃); the particles of this layer were very small in both the size and the vacancies between them; while the shapes were similar. However, some distortion of Al₃Ti particles in the case of AT-3 alloy was observed (Fig. 12c). Figure 12e exhibits the attack of corrosion on the specimen surface, which seemed to be deeper and more vigorous on the AT-4 alloy compared to that of AT-3. In addition, the pitting attack on the surface of AT-4 alloy was observed. Insoluble products of corrosion on the alloy AT-4 surface could slow down the corrosion processes compared to those of AT-3 alloy. This indicated that the resistance of corrosion on the mentioned electrode surface (AT-4) was higher compared to that of AT-3. Consequently, SEM supported

the data obtained from both polarization and EIS measurements.

Figure 13 exhibits photographs of Al and some investigated alloys (AT-3 and AT-4) after polarization experiments in 0.5 M H₃PO₄ solution. It appears from Fig. 13a that the Al surface was covered with the corrosion product, while the surface of the electrode could be barely seen. However, the layer formed on the surface as a result of H₃PO₄ (Fig. 13a) was less in size than that in the HCl solution (Fig. 12a). This means that the rate of corrosion in the H₃PO₄ solution was lower than that in HCl. Figure 13 (c and e) exhibits the corrosion product formed on the surface of AT-3 and AT-4 alloys, respectively. It is clear that the intensity of corrosion attack became lower compared to that of HCl solution; Al₃Ti particles could still be seen with a slight distortion occurring in H₃PO₄. On the other hand, the formation of the pits in the H₃PO₄ solution was not observed. This indicates that PO₄³⁻ ions became less aggressive compared to Cl⁻ ions.

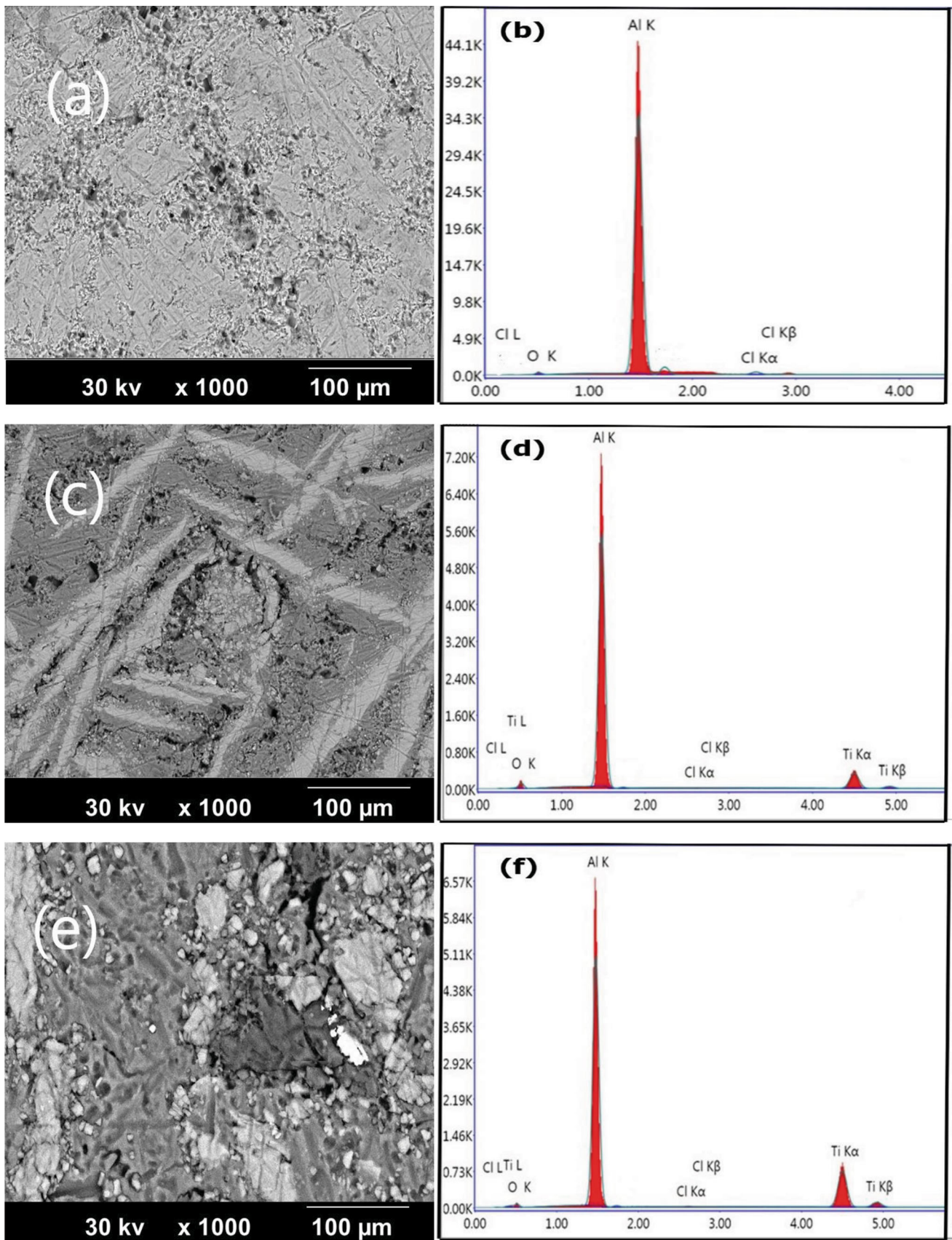


Fig. 12 Photographs of SEM and EDAX analysis of corrosion of specimen surface of (a, b) Al, (c, d) specimen AT-3, and (e, f) specimen AT-4 in 0.5 M HCl, magnified at 1000 times

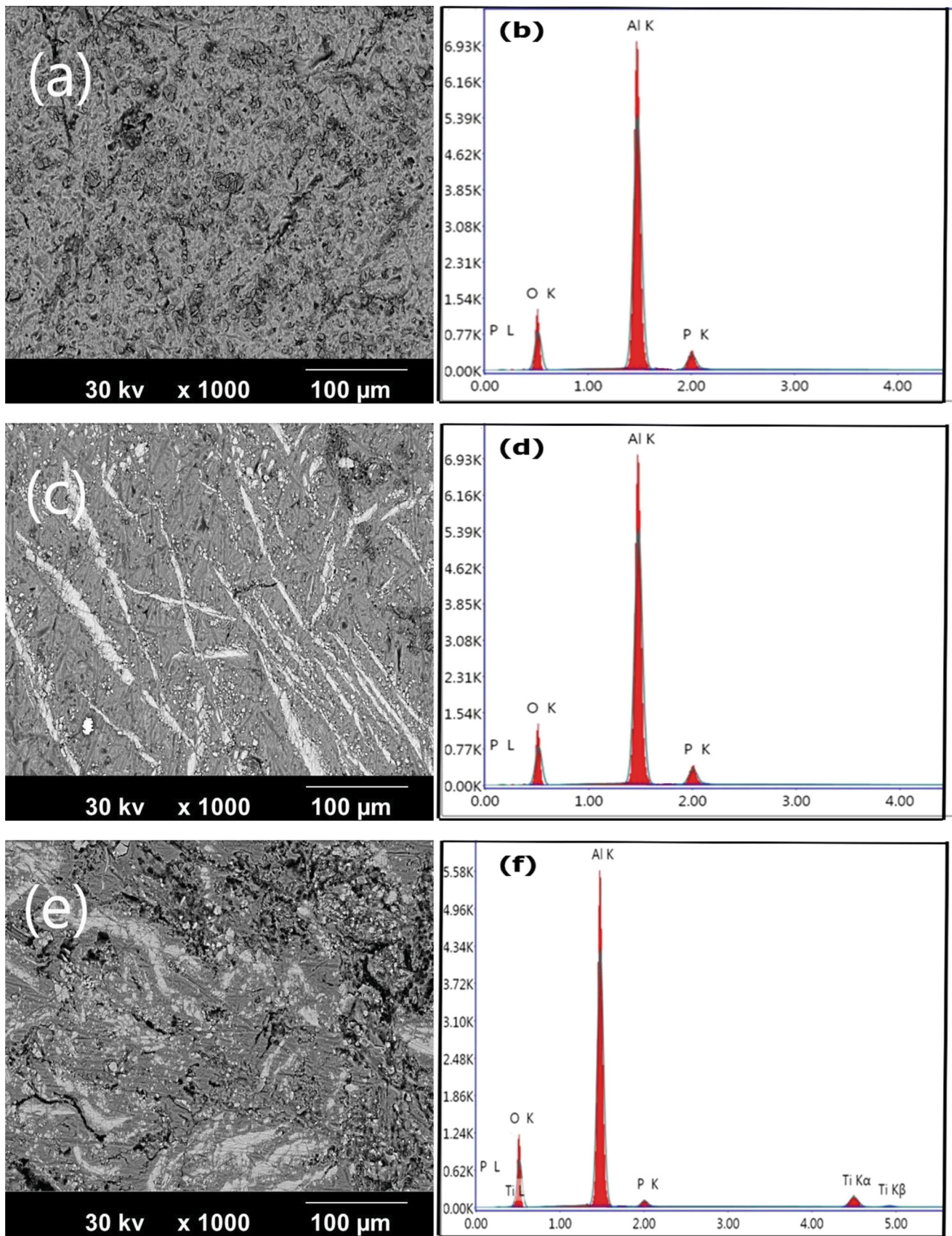


Fig. 13 Photographs of SEM and EDAX analysis of corrosion of specimen surface of (a, b) Al, (c, d) specimen AT-3, and (e, f) specimen AT-4 in 0.5 M H_3PO_4 , magnified at 1000 times

Table 11 EDAX data of Al and Al-Ti alloys substrates after immersion in 0.5 M solutions of HCl and H₃PO₄ by % weight with an accuracy $\pm 5.0\%$

Test	Sample's name	Elements, wt. %				
		Al	Ti	O	Cl	P
In the presence of 0.5 M HCl	Al	94.32	...	3.68	2	...
	AT-3	72.21	13.68	9.88	4.23	...
	AT-4	64.03	26.17	6.57	3.23	...
In the presence of 0.5 M H ₃ PO ₄	Al	61.78	...	31.07	...	7.15
	AT-3	56.82	6.4	28.48	...	8.3
	AT-4	53.24	8.24	30.32	...	8.2

EDAX data (Table 11) are detected the percent of elements and oxides in the products of corrosion, which are formed on Al and its investigated alloys surfaces at the active region (after the experiments of potentiodynamic polarization). The data in b, d, and f of Fig. 12 reveal that the percentage of Al decreases with the increasing addition of Ti to Al in HCl solution. On the other hand, the percentage of O and Cl elements increases on the alloy surface compared with that of Al. This indicates that the amount of both Cl and O elements in the corrosion products on the alloy surface is higher than that formed on the Al surface. But in the H₃PO₄ solution, the data of EDAX (Fig. 13b, d, and f) exhibit a slight decrease of Al with adding Ti, while a significant increase of O element of the studied electrodes in H₃PO₄ compared with that observed in HCl. This indicates that the higher O element which is detected in the corrosion products can be attributed to the presence of four oxygen atoms in PO₄³⁻ ion in addition to O of Al₂O₃. EDAX results supported the data obtained from potentiodynamic measurements.

4. Conclusions

Al-Ti alloy with various Ti contents was prepared using the melt method. The morphology and structure of the prepared alloys were studied with XRD and SEM. The data obtained showed the formation of Al₃Ti phase. The density functional theory (DFT) was used in the calculations of the experimental and theoretical HOMO-LUMO values. Electrochemical measurements of Al and Al-Ti alloy in 0.5 M solution for both HCl and H₃PO₄ were investigated using Tafel plot extrapolations and EIS techniques. The microhardness value increases with the addition of Ti to Al and is due to the formation of the Al₃Ti phase. The results revealed that the rate of corrosion increased with an increase of Ti amount in the specimen. The rate of corrosion of the investigated electrodes gradually increased with the raised temperature of the solution. This proved that the growth of oxide film on the surface of the studied electrode was impeded by a temperature increase in the electrolyte solution. The complex plane impedance plots of Al and its investigated alloys revealed the three-time constants. The first one was a loop of capacitive at high frequencies, the second one was a loop of inductive at medium frequencies, and the third constant was the second loop of capacitive at low frequencies. The values of thermodynamic parameters, such as E_a , ΔS , and ΔH of corrosion processes of the investigated electrodes in both HCl and H₃PO₄, were evaluated. The data obtained for both HCl and H₃PO₄ of all investigated electrodes exhibited that i_{corr} in H₃PO₄ solution was lower than that in HCl. This trend could

be attributed to the aggressive attack of Cl⁻ ions on each specimen surface. The data obtained from Tafel plots exhibited a trend similar to that observed from EIS measurements. SEM images confirmed that the corrosion rate on the surface after the potentiodynamic measurements was higher in HCl compared to that of H₃PO₄.

Funding

Open access funding provided by The Science, Technology & Innovation Funding Authority (STDF) in cooperation with The Egyptian Knowledge Bank (EKB).

Open Access This article is licensed under a Creative Commons Attribution 4.0 International License, which permits use, sharing, adaptation, distribution and reproduction in any medium or format, as long as you give appropriate credit to the original author(s) and the source, provide a link to the Creative Commons licence, and indicate if changes were made. The images or other third party material in this article are included in the article's Creative Commons licence, unless indicated otherwise in a credit line to the material. If material is not included in the article's Creative Commons licence and your intended use is not permitted by statutory regulation or exceeds the permitted use, you will need to obtain permission directly from the copyright holder. To view a copy of this licence, visit <http://creativecommons.org/licenses/by/4.0/>.

References

1. C. Vargel, Corrosion of Aluminium. Elsevier Ltd, ed., Oxford, ISBN 0-080-33395-4, (2004)
2. B. Davó and J.J. De Damborenea, Use of Rare Earth Salts as Electrochemical Corrosion Inhibitors for an Al-Li-Cu (8090) Alloy in 3.56% NaCl, *Electrochim. Acta*, 2004, **49**(27), p 4957-4965
3. S. Caporali, A. Fossati, A. Lavacchi, I. Perissi, A. Tolstogousov, and U. Bardi, Aluminium Electroplated from Ionic Liquids as Protective Coating Against Steel Corrosion, *Corros. Sci.*, 2008, **50**(2), p 534-539
4. H.-C. Fang, K.-H. Chen, Z. Zhang, and C.-J. Zhu, Effect of Yb Additions on Microstructures and Properties of 7A60 Aluminum Alloy, *Trans. Nonferrous Metals Soc. China*, 2008, **18**(1), p 28-32
5. R. Rosliza, W.B.W. Nik, and H.B. Senin, The Effect of Inhibitor on the Corrosion of Aluminum Alloys in Acidic Solutions, *Mater. Chem. Phys.*, 2008, **107**(2-3), p 281-288
6. J.B. Bessone, The Activation of Aluminium by Mercury Ions in Non-aggressive Media, *Corros. Sci.*, 2006, **48**(12), p 4243-4256
7. I. Gurrappa, Cathodic Protection of Cooling Water Systems and Selection of Appropriate Materials, *J. Mater. Process. Technol.*, 2005, **166**(2), p 256-267

8. C.F. Schrieber and J.T. Reding, Field Testing a New Aluminum Anode Al-Hg-Zn Galvanic Anode for Sea Water Applications, *Mater. Prot.*, 1967, **6**(5), p 33-36
9. Y.U. Huashun, C. Hongmei, S. Liming, and M. Guanghui, Preparation of Al-Al₃Ti in Situ Composites by Direct Reaction Method, *Rare Met.*, 2006, **25**(1), p 32-36
10. A.A. Ghoneim, M.A. Ameer, and A.M. Fekry, Electrochemical Behavior of Al-Si Alloy in Phosphoric Acid Containing Halogen or Oxyhalogen Anions, *Int J Electrochem Sci*, 2012, **7**(7), p 10851-10864
11. C.B. Spainhour, Phosphoric Acid, *Encyclopedia of Toxicology (Third Edition)*. P. Wexler Ed., Academic Press, Cambridge, 2014, p 916-919
12. M.A. Amin, Q. Mohsen, and O.A. Hazzazi, Synergistic Effect of I⁻ Ions on the Corrosion Inhibition of Al in 1.0 M Phosphoric acid Solutions by Purine, *Mater. Chem. Phys.*, 2009, **114**(2-3), p 908-914
13. H. Ashassi-Sorkhabi, B. Shabani, B. Aligholipour, and D. Seifzadeh, The Effect of Some Schiff Bases on the Corrosion of Aluminum in Hydrochloric Acid Solution, *Appl. Surf. Sci.*, 2006, **252**(12), p 4039-4047
14. T. Ai, F. Liu, X. Feng, Q. Yu, N. Yu, M. Ruan, X. Yuan, and Y. Zhang, Processing, Microstructural Characterization and Mechanical Properties of in Situ Ti₃AlC₂/TiAl₃ Composite by hot Pressing, *Mater. Sci. Eng., A*, 2014, **610**, p 297-300
15. A. Rohatgi, D.J. Harach, K.S. Vecchio, and K.P. Harvey, Resistance-curve and Fracture Behavior of Ti-Al₃Ti Metallic-intermetallic Laminate (MIL) Composites, *Acta Mater.*, 2003, **51**(10), p 2933-2957
16. H. Sato, T. Murase, T. Fujii, S. Onaka, Y. Watanabe, and M. Kato, Formation of a Wear-induced Layer with Nanocrystalline Structure in Al-Al₃Ti Functionally Graded Material, *Acta Mater.*, 2008, **56**(17), p 4549-4558
17. L. Jiao, Y.T. Zhao, Y. Wu, S. Zhang, and X.L. Wang, Microstructure of In Situ Synthesized Al₃Ti/6063 under Combination of Magnetic Fields, (2012), **600**, 199-203
18. D.-Y. Yang, S. Guo, H.-X. Peng, F.-Y. Cao, N. Liu, and J.-F. Sun, Size Dependent Phase Transformation in Atomized TiAl Powders, *Intermetallics*, 2015, **61**, p 72-79
19. I. Dinaharan, G.A. Kumar, S.J. Vijay, and N. Murugan, Development of Al₃Ti and Al₃Zr Intermetallic Particulate Reinforced Aluminum Alloy AA6061 in Situ Composites Using Friction Stir Processing, *Mater. Des.*, 2014, **63**, p 213-222
20. J.B. Al-Dabbagh, R.M. Tahar, and S.A. Harun, Structural and Phase Formation of TiAl Alloys Synthesized by Mechanical Alloying and Heat Treatment, *Int. J. Nanoelectron. Mater.*, 2015, **8**, p 23-32
21. M. Ismael, A. Abdou, and A.M. Abdel-Mawgoud, Synthesis, Characterization, Modeling, and Antimicrobial Activity of FeIII, CoII, NiII, CuII, and ZnII Complexes Based on Tri-substituted Imidazole Ligand, *Z. Für Anorg. Und Allg. Chem.*, 2018, **644**(20), p 1203-1214
22. M. Ismael, A.-M.M. Abdel-Mawgoud, M.K. Rabia, and A. Abdou, Design and Synthesis of Three Fe (III) Mixed-Ligand Complexes: Exploration of Their Biological and Phenoxazinone Synthase-like Activities, *Inorg. Chim. Acta*, 2020, **505**, 119443
23. A.-R. El-Sayed, H.S. Mohran, and H.M. Abd El-Lateef, Corrosion Study of Zinc, Nickel, and Zinc-nickel Alloys in Alkaline Solutions by Tafel Plot and Impedance Techniques, *Metallur. Mater. Trans. A*, 2012, **43**(2), p 619-632
24. V. Goyal, R. Ravi, S.R. Bakshi, and P.R. Soni, Development and Mechanical Properties of In Situ Al₃Ti-Reinforced Nanostructured AA6061 via Mechanical Alloying, *J. Mater. Eng. Perform.*, 2019, **28**(1), p 117-122
25. H. Al-Ethari, A.H. Haleem, and M.H. Hassan, Comparative Study to the Effect of Mold Vibration and Addition of Titanium on Microstructure, Hardness, Dendrite Grain Size and Porosity of Al-Si Eutectic, (2020)
26. A.H. Seikh, E.-S.M. Sherif, S.M.A. Khan Mohammed, M. Baig, M.A. Alam, and N. Alharthi, Microstructure Characterization and Corrosion Resistance Properties of Pb-Sb Alloys for Lead Acid Battery Spine Produced by Different Casting Methods, *PLoS ONE*, 2018, **13**(4), p e0195224
27. A.-R. El-Sayed, H.S. Mohran, and H.M. Abd El-Lateef, Effect of Minor Nickel Alloying with Zinc on the Electrochemical and Corrosion Behavior of Zinc in Alkaline Solution, *J. Power Sour.*, 2010, **195**(19), p 6924-6936
28. H.S. Mohran, A.-R. El-Sayed, and H.M. Abd El-Lateef, Hydrogen Evolution Reaction on Sn, In, and Sn-In Alloys in Carboxylic Acids, *J. Solid State Electrochem.*, 2009, **13**(8), p 1147-1155
29. M. Ismael, A.-M.M. Abdel-Mawgoud, M.K. Rabia, and A. Abdou, Ni (II) Mixed-ligand Chelates Based on 2-hydroxy-1-naphthaldehyde as Antimicrobial Agents: Synthesis, Characterization, and Molecular Modeling, *J. Mol. Liq.*, 2021, **330**, 115611
30. M. Ismael, A.-M.M. Abdel-Mawgoud, M.K. Rabia, and A. Abdou, Synthesis, Characterization, Molecular Modeling and Preliminary Biochemical Evaluation of New Copper (II) Mixed-ligand Complexes, *J. Mol. Struct.*, 2021, **1227**, 129695
31. R.A. Majed, M. Mahdi, H.A. Al-Kaisy, and S.A.A. Maged, Corrosion Behavior for Al-Cu-Mg Alloy by Addition of SiO₂ Particles in Seawater, *Eng. Technol. J.*, 2014, **32**(2), p 354-364
32. V. Branzoi, F. Golgovici, and F. Branzoi, Aluminium Corrosion in Hydrochloric Acid Solutions and the Effect of Some Organic Inhibitors, *Mater. Chem. Phys.*, 2003, **78**(1), p 122-131
33. S.M. Traldi, J.L. Rossi, and I. Costa, An Electrochemical Investigation of the Corrosion Behavior of Al-Si-Cu Hypereutectic Alloys in Alcoholic Environments. *Revista de Metalur.*, 86-90, (2003)
34. H.S. Mohran, A.-R. El-Sayed, and H.M. Abd El-Lateef, Anodic Behavior of Tin, Indium, and Tin-indium Alloys in Oxalic Acid Solution, *J. Solid State Electrochem.*, 2009, **13**(8), p 1279-1290
35. M. Stern and A.L. Geary, A Theoretical Analysis of the Shape of Polarization Curves, *J. Electrochem. Soc.*, 1957, **104**(1), p 56-63
36. W. Taro and D. Landolt, Electrochemical Determination of the Porosity of Single and Duplex PVD Coatings of Titanium and Titanium Nitride on Brass, *J. Electrochem. Soc.*, 1998, **145**(12), p 4173
37. S.H. Ahn, Y.S. Choi, J.G. Kim, and J.G. Han, A Study on Corrosion Resistance Characteristics of PVD Cr-N Coated Steels by Electrochemical Method, *Surf. Coat. Technol.*, 2002, **150**(2-3), p 319-326
38. H.M. Abd El-Lateef, E.-S. Abdel-Rahman, and H.S. Mohran, Role of Ni Content in Improvement of Corrosion Resistance of Zn-Ni Alloy in 3.5% NaCl Solution Part I: Polarization and Impedance Studies, *Trans. Nonferrous Metals Soc. China*, 2015, **25**(8), p 2807-2816
39. M. Šeruga and D. Hasenay, Electrochemical and Surface Properties of Aluminium in Citric Acid Solutions, *J. Appl. Electrochem.*, 2001, **31**(9), p 961-967
40. S. Deng, X. Li, and G. Du, An Efficient Corrosion Inhibitor of Cassava Starch Graft Copolymer for Aluminium in Phosphoric Acid, *Chin. J. Chem. Eng.*, 2020 <https://doi.org/10.1016/j.cjche.2020.08.013>
41. X. Wang, A. Jha, and R. Brydson, In Situ Fabrication of Al₃Ti Particle Reinforced Aluminium Alloy Metal-matrix Composites, *Mater. Sci. Eng., A*, 2004, **364**(1-2), p 339-345
42. W. Lu, L. Li, and L. Huang, *Casting alloys and their melting*, ed., China Machine Press, Beijing, 2002
43. P.D. Sequeira, Y. Watanabe, and Y. Fukui, Backward Extrusion of Al-Al₃Ti Functionally Graded Material: Volume Fraction Gradient and Anisotropic Orientation of Al₃Ti Platelets, *Scripta Mater.*, 2005, **53**(6), p 687-692
44. S.K. Das, Al-rich Intermetallics in Aluminum Alloys, *Intermetallic Compounds. Structural Application of Intermetallic Compounds*, Wiley, New York, **3**, 179-181, (2000)
45. E.E. Oguzie, B.N. Okolue, E.E. Ebenso, G.N. Onuoha, and A.I. Onuchukwu, Evaluation of the Inhibitory Effect of Methylene Blue Dye on the Corrosion of Aluminium in Hydrochloric Acid, *Mater. Chem. Phys.*, 2004, **87**(2-3), p 394-401
46. R.T. Foley and T.H. Nguyen, The Chemical Nature of Aluminum Corrosion: V. Energy Transfer in Aluminum Dissolution, *J. Electrochem. Soc.*, 1982, **129**(3), p 464
47. H.M. Abd El-Lateef, A.-R. El-Sayed, H.S. Mohran, and H.A.S. Shilkamy, Corrosion Inhibition and Adsorption Behavior of Phytic Acid on Pb and Pb-In Alloy Surfaces in Acidic Chloride Solution, *Int. J. Ind. Chem.*, 2019, **10**(1), p 31-47
48. I.B. Obot, N.O. Obi-Egbedi, S.A. Umoren, and E.E. Ebenso, Synergistic and Antagonistic Effects of Anions and IPOMOEA INVULCRATA as Green Corrosion Inhibitor for Aluminium Dissolution in Acidic Medium, *Int. J. Electrochem. Sci*, 2010, **5**(7), p 994-1007
49. A.-R. El-Sayed, H.S. Mohran, and H.M. Abd El-Lateef, The Inhibition Effect of 2, 4, 6-tris (2-pyridyl)-1, 3, 5-triazine on Corrosion of Tin, Indium and Tin-indium Alloys in Hydrochloric Acid Solution, *Corros. sci.*, 2010, **52**(6), p 1976-1984
50. M.T. Alhaffar, S.A. Umoren, I.B. Obot, and S.A. Ali, Isoxazolidine Derivatives as Corrosion Inhibitors for Low Carbon Steel in HCl Solution: Experimental, Theoretical and Effect of KI Studies, *RSC Adv.*, 2018, **8**(4), p 1764-1777

51. E.C. Ogoko, S.A. Odoemelam, B.I. Ita, and N.O. Eddy, Adsorption and Inhibitive Properties of Clarithromycin for the Corrosion of Zn in 0.01 to 0.05 M H₂SO₄, *Port. Electrochim. Acta*, 2009, **27**(6), p 713-724
52. M. Bouklah, B. Hammouti, M. Benkaddour, and T. Benhadda, Thiophene Derivatives as Effective Inhibitors for the Corrosion of Steel in 0.5 m H₂SO₄, *J. Appl. Electrochem.*, 2005, **35**(11), p 1095-1101
53. E.E. Oguzie, Corrosion Inhibition of Aluminium in Acidic and Alkaline Media by Sansevieria Trifasciata Extract, *Corros. Sci.*, 2007, **49**(3), p 1527-1539
54. K.K. Al-Neami, A.K. Mohamed, I.M. Kenawy, and A.S. Fouda, Inhibition of the Corrosion of Iron by Oxygen and Nitrogen Containing Compounds, *Monatshfte Für Chemie/Chem. Mon.*, 1995, **126**(4), p 369-376
55. S.S. Abd El-Rehim, M.A.M. Ibrahim, and K.F. Khaled, 4-Aminoantipyrine as an Inhibitor of Mild Steel Corrosion in HCl Solution, *J. Appl. Electrochem.*, 1999, **29**(5), p 593-599
56. A.-R. El-Sayed, H.S. Mohran, and H.M. Abd El-Lateef, Effect of Some Nitrogen-heterocyclic Compounds on Corrosion of Tin, Indium, and their Alloys in HClO₄, *Monatshfte Für Chemie-Chem. Mon.*, 2012, **143**(1), p 51-64
57. J. Bessone, C. Mayer, K. Jüttner, and W.J. Lorenz, AC-impedance Measurements on Aluminium Barrier type Oxide Films, *Electrochim. Acta*, 1983, **28**(2), p 171-175
58. C.M.A. Brett, On the Electrochemical Behaviour of Aluminium in Acidic Chloride Solution, *Corros. Sci.*, 1992, **33**(2), p 203-210
59. G.T. Burstein and R.J. Cinderey, The Potential of Freshly Generated Metal Surfaces Determined from the Guillotined Electrode—A New Technique, *Corros. Sci.*, 1991, **32**(11), p 1195-1211
60. M. Metikoš-Huković, R. Babić, and Z. Grubač, Corrosion Protection of Aluminium in Acidic Chloride Solutions with Nontoxic Inhibitors, *J. Appl. Electrochem.*, 1998, **28**(4), p 433-439
61. H.J.W. Lenderink, M.V.D. Linden, and J.H.W. De Wit, Corrosion of Aluminium in Acidic and Neutral Solutions, *Electrochim. Acta*, 1993, **38**(14), p 1989-1992
62. E.A. Noor, Evaluation of Inhibitive Action of Some Quaternary N-heterocyclic Compounds on the Corrosion of Al-Cu Alloy in Hydrochloric Acid, *Mater. Chem. Phys.*, 2009, **114**(2-3), p 533-541
63. T. Våland and K.E. Heusler, Reactions at the Oxide-electrolyte Interface of Anodic Oxide Films on Aluminum, *J. Electroanal. Chem. Interfacial Electrochem.*, 1983, **149**(1-2), p 71-82
64. A.K. Singh and M.A. Quraishi, Effect of Cefazolin on the Corrosion of Mild Steel in HCl Solution, *Corros. Sci.*, 2010, **52**(1), p 152-160
65. S.S. Abd El Rehim, H.H. Hassan, and M.A. Amin, Corrosion Inhibition of Aluminum by 1, 1 (Lauryl amido) Propyl Ammonium Chloride in HCl Solution, *Mater. Chem. Phys.*, 2001, **70**(1), p 64-72
66. J.B. Bessone, D.R. Salinas, C.E. Mayer, M. Ebert, and W.J. Lorenz, An EIS Study of Aluminium Barrier-type Oxide films Formed in Different Media, *Electrochim. Acta*, 1992, **37**(12), p 2283-2290
67. M. Lebrini, M. Lagrenée, H. Vezin, M. Traisnel, and F. Bentiss, Experimental and Theoretical Study for Corrosion Inhibition of Mild Steel in Normal Hydrochloric Acid Solution by some New Macrocyclic Polyether Compounds, *Corros. Sci.*, 2007, **49**(5), p 2254-2269
68. M.A. Jingling, W. Jiuba, L.I. Gengxin, and X.V. Chunhua, The Corrosion Behaviour of Al-Zn-In-Mg-Ti Alloy in NaCl Solution, *Corros. Sci.*, 2010, **52**(2), p 534-539
69. X. Li, S. Deng and H. Fu, Sodium Molybdate as a Corrosion Inhibitor for Aluminium in H₃PO₄ Solution, *Corros. Sci.*, 2011, **53**(9), p 2748-2753
70. L. Jiao, Y.T. Zhao, Y. Wu, S. Zhang, and X.L. Wang, Microstructure of In Situ Synthesized Al₃Ti/6063 under Combination of Magnetic Fields. *Trans Tech Publ*, pp 199-203, (2012)
71. K. Zhang, J. Lu, J. Li, D. Zhang, L. Gao, and Y. Wang, A Novel Approach for Copper Protection: UV Light Triggered Preparation of the Click-assembled Film on Copper Surface, *Chem. Eng. J.*, 2020, **385**, 123406
72. X. Li and S. Deng, Inhibition Effect of Dendrocalamus Brandisii Leaves Extract on Aluminum in HCl, H₃PO₄ Solutions, *Corros. Sci.*, 2012, **65**, p 299-308
73. D. Prabhu and P. Rao, Coriandrum Sativum L.—A Novel Green Inhibitor for the Corrosion Inhibition of Aluminium in 1.0 M Phosphoric Acid Solution, *J. Environ. Chem. Eng.*, 2013, **1**(4), p 676-683
74. B. Xu, W. Yang, Y. Liu, X. Yin, W. Gong, and Y. Chen, Experimental and Theoretical Evaluation of Two Pyridinecarboxaldehyde Thiosemicarbazone Compounds as Corrosion Inhibitors for Mild Steel in Hydrochloric Acid Solution, *Corros. Sci.*, 2014, **78**, p 260-268

Publisher's Note Springer Nature remains neutral with regard to jurisdictional claims in published maps and institutional affiliations.